

ICSO 2016

International Conference on Space Optics

Biarritz, France

18–21 October 2016

Edited by Bruno Cugny, Nikos Karafolas and Zoran Sodnik



CMOS detectors: lessons learned during the STC stereo channel preflight calibration

E. Simioni

A. De Sio

V. Da Deppo

G. Naletto

et al.



icso proceedings



CMOS DETECTORS: LESSONS LEARNED DURING THE STC STEREO CHANNEL PREFLIGHT CALIBRATION

E. Simioni¹, A. De Sio², V. Da Deppo^{1,3}, G. Naletto^{4,1}, G. Cremonese³

¹CNR-Institute for Photonics and Nanotechnologies Padova, Via Trasea, 7 -35131 Padova, Italy. ²Dept. of Physics and Astronomy - Università degli Studi di Firenze, Largo E. Fermi 2, 50125 Firenze, Italy. ³INAF Astronomical Observatory Padova, Vicolo Osservatorio 5, Padova, Italy. ⁴Department of Information Engineering (DEI), University of Padova, Via Gradenigo 6/B-35131 Padova, Italy.

ABSTRACT

The Stereo Camera (STC), mounted on-board the BepiColombo spacecraft, will acquire in push frame stereo mode the entire surface of Mercury. STC will provide the images for the global three-dimensional reconstruction of the surface of the innermost planet of the Solar System. The launch of BepiColombo is foreseen in 2018. STC has an innovative optical system configuration, which allows good optical performances with a mass and volume reduction of a factor two with respect to classical stereo camera approach. In such a telescope, two different optical paths inclined of $\pm 20^\circ$, with respect to the nadir direction, are merged together in a unique off axis path and focused on a single detector. The focal plane is equipped with a 2k x 2k hybrid Si-PIN detector, based on CMOS technology, combining low read-out noise, high radiation hardness, compactness, lack of parasitic light, capability of snapshot image acquisition and short exposure times (less than 1 ms) and small pixel size (10 μm).

During the preflight calibration campaign of STC, some detector spurious effects have been noticed.

Analyzing the images taken during the calibration phase, two different signals affecting the background level have been measured. These signals can reduce the detector dynamics down to a factor of 1/4th and they are not due to dark current, stray light or similar effects.

In this work we will describe all the features of these unwilling effects, and the calibration procedures we developed to analyze them.

I. INTRODUCTION

BepiColombo (BC) is a mission devoted to the study of the planet Mercury. It is a joint mission of the European Space Agency (ESA) and the Japan Aerospace eXploration Agency (JAXA), scheduled for launch towards the beginning of 2018 [1].

The BC spacecraft is composed of three different modules: one is the propulsion system needed to transfer the scientific payloads to Mercury, the other two modules. i.e. the Mercury Planetary Orbiter (MPO) and the Mercury Magnetospheric Orbiter (MMO), are carrying the scientific instrumentation [2].

SIMBIO-SYS [3], an integrated suite including a high resolution camera (HRIC), a stereo camera (STC) and a visible and near infrared spectrometer (VIHI), is mounted on the BC MPO module.

The main scope of STC is the 3D global mapping of the Mercury surface with a vertical accuracy requirement of 80/90 m at perihelion [4]. The channel is equipped with some filters in order to select specific wavelength ranges. There are different glass filtering strips glued together to form a single substrate, which is then mounted in front of the detector (see Fig. 1) [5].

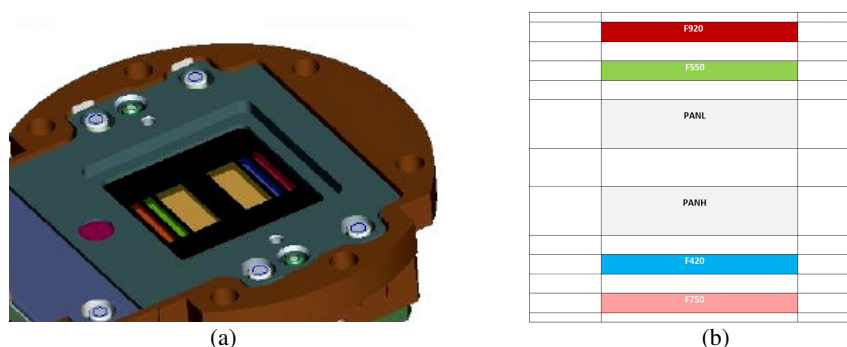


Fig. 1. In (a), schematics of the FPA housing with the FSA structure clearly visible (Courtesy of Raytheon Vision Systems). The two panchromatic larger filter areas are at the center, the smaller broadband ones towards the edges. Definitions of the filter with respect to their central wavelength are shown in (b).

The two panchromatic filters are centered at 700 nm, with 200 nm of bandwidth, and they are dedicated to acquisitions needed for the 3D reconstruction (stereo mapping operation mode). There are also four broadband

BB filters (20 nm bandwidth), which cover the wavelengths from the visible to the near infrared, used to study the Mercury surface composition in specific areas.

The operation strategy of STC foresees two different phases: the Global Mapping (GM) phase and the Color Mapping (CM) one. In the GM phase panchromatic filters are used to cover all the planet surface. The smearing due to spacecraft velocity and the linearity of the filters, limited to 0.3 ms at perihelion, obliged in this phase the use of high Repetition Time (RT) (7/12 s) and low Integration Time IT (<2ms). Different strategy is assumed in CM phase in which shorter swath and low sensibility of the BB filters impose low RT(1/2s) to guarantee image overlapping and high IT(<100ms).

Due to its orbit in close proximity to the Sun, BepiColombo instruments will work in a harsh environment due to radiation dose and heat production. Thus, a CMOS has been chosen as detector for STC thanks to its intrinsic radiation hardness and good performances at high temperatures.

For CMOS APS detector the readout of the charge from each pixel is done by a readout electronics integrated into the pixel itself. Moreover its capability to direct download only specific pixels of the whole FPA allows to select six specific windows, corresponding for instance to the areas of each filter. This also permits to acquire a small area outside the illuminated part to be used as dark current monitor, and to reduce the readout time and the dimensions of the buffer/data storage unit. Finally, the fast readout allows both to avoid the presence of mechanical shutters and to achieve short exposition times (even less than 1 ms) that are necessary for a mission to Mercury.

The detector has been developed by Raytheon Vision Systems (RVS) that has produced a custom visible sensor based on a 2048 × 2048 format with a 10 μm pitch unit cell [6]. The same device has been selected also for the SIMBIO-SYS HRIC [7] and for the Colour and Stereo Surface Imaging System (CaSSIS) for the ExoMars mission [8].

The sensor was designed to achieve high sensitivity as well as low input noise (<100 e-) for space-based, low light conditions. It also must maintain performance parameters in a total ionizing dose environment up to 70 kRad (Si) as well as immunity to Single Event Effects, such as latch up and single event upset.

Pre-flight calibration of the STC, in particular radiometric [9], geometrical [10], spectral and stereo validation ([11],[12],[13]) calibrations were performed in Leonardo S.p.a. facilities to provide an adequate characterization of the STC flight model for its future scientific use.

The radiometric calibration campaign has been performed with the scope to define for each pixel the dark curve, the radiometric response, including the linearity and saturation limits.

During these calibrations of both Spare and Flight Focal Plane Assembly (FPA), some unidentified (unexpected) effects have been noticed, i.e. charging effects and anomalies into the Dark Signal Non Uniformity (DSNU). These phenomena are modifying the response of the detector and reducing the dynamic range of the measurements.

In this work the effects are described starting from the acquired data. Then we will do the phenomenological analyses in order to discriminate different contributors and to characterize each of them. Finally, we will discuss these sensor phenomena from the perspective of their use in the context of STC Stereo Camera.

II. DETECTOR AND READOUT INTEGRATED CIRCUIT DESIGN

The use of a hybrid configuration allows to take benefits from both a high quality material, especially developed for high quantum efficiency (92%) in a wide spectral range (8% of spectral flatness up to NIR) with a 100% filling factor. A fast and high performances CMOS Readout Integrated Circuit (ROIC) enables an architecture which combines the ability to readout multiple windows through a single analog output, with a power budget of 120 mW. The detector and ROIC are fabricated separately, then bonded together to form a single hybrid structure. In Fig. 2 the structure of the FPA is reported as well as the structure of the bonding between the SI-PIN layer and the ROIC.

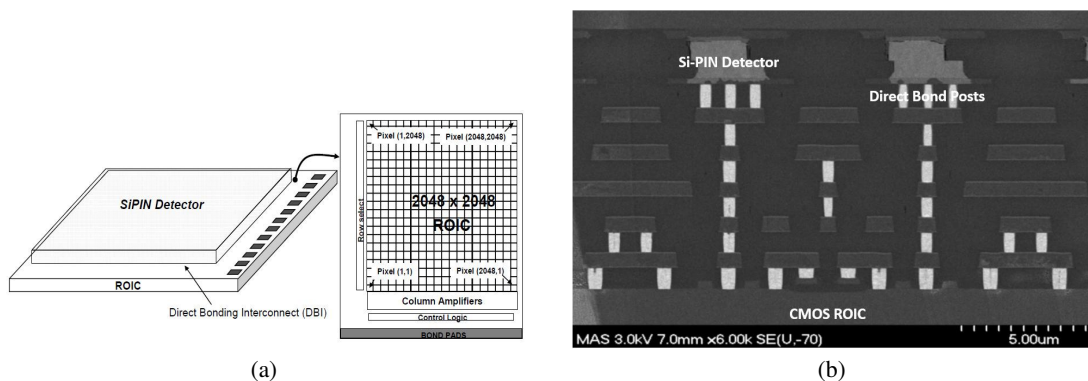


Fig. 2. In (a) block diagram of the ROIC and the detector. In (b) SEM of high density Direct Bond Interconnect showing, unlike traditional indium bump solution, no air gap between detector and ROIC. In the image five layers of metal can be identify.

In the Tab. 1 some of the characteristics of the detector are reported.

Tab. 1. Main detector and ROIC characteristics.

Sensor dimensions	2048x2048 px ²	Fill Factor	100%	Read out Noise (RMS)	60 e-
Unit Cell	10x10 μm ²	Spectral Flatness	8% (@NIR)		10 DN(@268K)
Min. Window	128x64 px ²	Quantum efficiencies	92%	Charge conversion	14 μV/e-
Max. N windows	6 windows	FPA power budget	120 mW	Integration Time range	0.04 to 5000 ms
A/D Conversion	14 bit	Analog output velocity	<5 Mpps	Operating temperature	213.15- 313.15K

Instead of the traditional indium bumps deposited on both the detector and the ROIC to hybridize the two surfaces together, RVS has developed a novel oxide bond interconnect solution whit extremely high interconnect yield. Such a technology has the advantage to leave no air gap between the detector and the ROIC and the bind between the two pieces has less tensions. Tensions can induce bonding breaks if subjected to cyclic thermal gradients. ROIC basic design incorporates as well an integrate-then read (ITR) operation at the maximum output rate of 5 Mpps. This strategy permits, through the use of the four transistor unit cell, to perform RESET phase (in which the charge accumulated before on the pixel is cleaned) and then to realize the simultaneous integration of photocurrent on all pixels.

III. DATA ANALISYS

A. Effects identification

As it happened in SWAP telescope (CMOS based) calibration [14], the FPA calibration for STC highlighted some unexpected phenomena in the detector behaviour not correlated with dark or photonic signals. These effects can be identified acquiring sequences of images, Fig. 3 reports two examples and the measured value (in Digital Number (DN) units) of a randomly chosen pixel is plotted versus the sequential number of the acquisition. In particular two sequences are reported, each of them represents a sets of 15 images taken in dark condition at the nominal detector temperature of 268K. Each set of 15 images is characterized by the same integration time (IT) and a constant RT (0.7s). Such IT grows between one set and the following one.

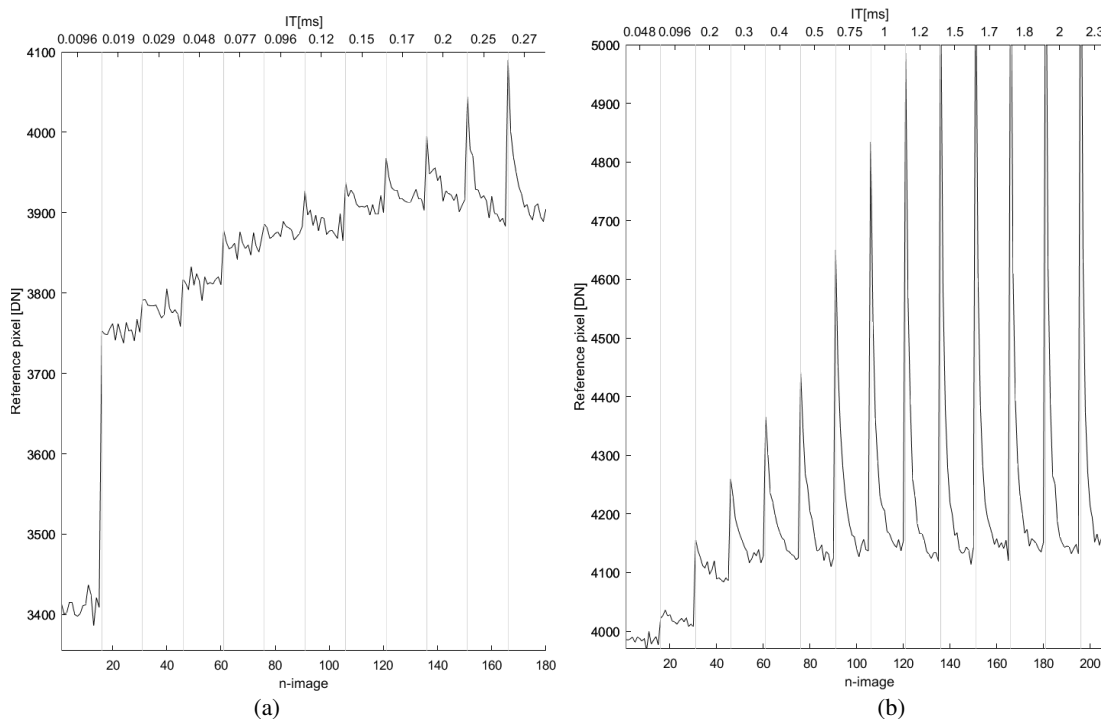


Fig. 3. Signal on the reference pixel for sets of images acquired with progressively increased IT. In (a) the pixel measured values for 180 images (12 sets) are shown. The IT of each set is reported in the upper X axis and it ranges between 0.0048 ms and 0.27 ms. In (b) the pixel values for 210 images (14 sets) acquired with longer IT (up to 2.3 ms) are plotted. Both the sequences have been acquired at 268K detector temperature.

These images have been acquired without illumination, thus they should be affected only by Dark Current (DC) and Fixed Pattern Noise (FPN). Since the IT is limited up to few ms, the DC contribution should be negligible. It is then clear that a spurious signal of thousands of DN is present and its value is stabilized during each set of pictures (i.e. the signal decreases after the peaks in Fig. 3b). So, from these graphs, we can state that at least two different spurious effects are present:

- a steep growth of the background signal: we called it Pedestal Effect (PE).
- a Peak Offset (PO) in the DN values of the pixel in the first image of each set.

The PE cannot be correlated with DC. DC is, in fact, caused by the statistical transitions of electrons in conduction band due to thermal energy, and so DC must be linear with integration time. The growth of this background (PE) is steeper and it seems to reach a saturation level.

PO seems to have a different origin. The effect is high but decreases every time a new image is acquired into the same set (same integration time) of the sequence bringing the signal to the Pedestal level. Such an effect occurs every time a certain time elapses between two images.

In order to find a phenomenological model to fit the detector behaviour and to mitigate these effects, accurate analyses of the data will be carried out. Specific sets of images have been considered to highlight the specific aspects of the effects.

IV. MODELS PROPOSED

A. The Pedestal Effect (PE)

Such a pedestal starts to build up at really short ITs and it reaches its maximum for an IT of 0.4 ms. So, all images with $IT < 0.4$ ms are affected by a non constant PE.

It seems that the build up of the PE is not affected by the time elapsed since the previous image. For $IT > 0.4$ ms the PE is constant (in the limits of the RON) and, subtracting its measured value for each pixel, it is possible to evaluate the correct value of the dark or light signal.

In order to avoid contribution by the PO, we select some pixels and we considered only the value of the pixel in the last image of each sequence. This value has been analysed with respect to the IT. The behaviour has been fitted with an exponential decay as represented in Eq (1):

$$y(t) = y_0 - Ae^{-\frac{t}{\tau}} \quad (1)$$

The comparison between the measurements and the model is shown in Fig. 4.

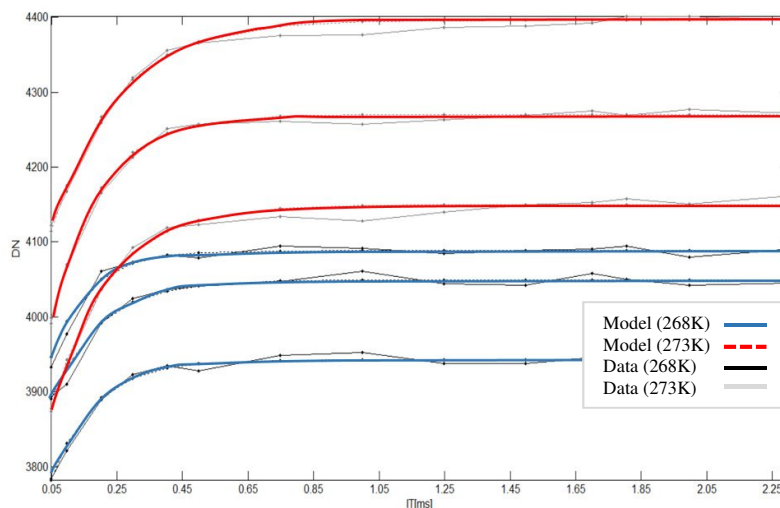


Fig. 4. This picture represents data extracted from the same series of Fig. 3b, each characterised by different integration times. The values of 3 reference pixels are shown demonstrating the variability of the FPN. Lighter curves are representative of high temperature data (273K) while darker of nominal temperature (268K). The values grow rapidly up to a saturation level. Dotted lines represent the model used to fit the behaviour.

Such an analysis, done for one pixel, can be extended to more pixels, more detector areas to have a better statistic. It can be used also to identify the spatial distribution of PE. The fitting procedure has been applied separately to each pixel, to be able to study the consistency of the model as well as the statistical distribution of the data. The results of these operations are reported in Fig. 5. The data used for this analysis have been acquired at two different detector temperatures: 268K and 273K. The mean results of the fitting analysis are reported in Tab. 2.

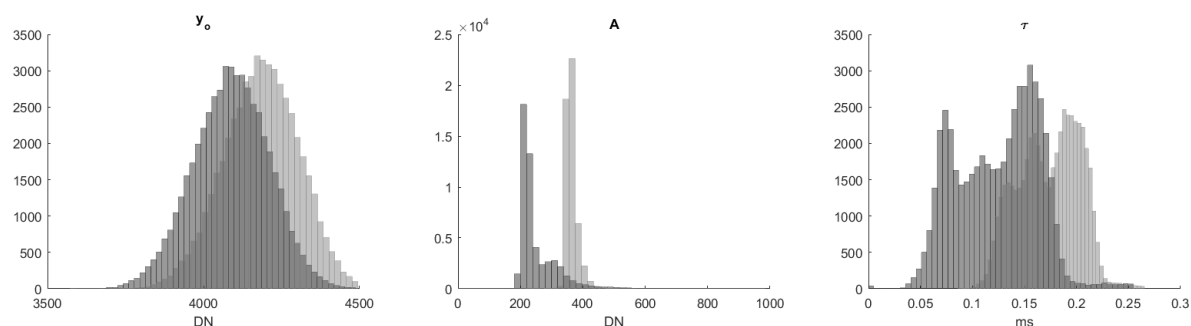


Fig. 5. The figure shows the distribution of the three parameter values defining the model for two different detector temperatures: in dark grey 268K in grey 273K. From the left side, the parameters represented are: the asymptotic value y_o , the exponential amplitude A and the temporal exponential decay constant τ .

Tab. 2. The table shows the mean values of the model parameters as well as the mean accuracy of the fitting defined for each pixel of the detector at two different detector temperatures. Fitting errors result in the limits of the RON (10 DN). Confidence bounds are considered at 95%.

Parameters	y_o [DN]	A [DN]	Tau [ms]	Accuracy [DN]
Mean Value (268K)	4088	254	0.12	9.0
Mean Value (273K)	4184	363	0.17	8.3
Coefficients bounds (%)	0.09	11.7	6.7	

The consistency of this fitting model is underlined by the coefficient of determination R of the fit and by the distribution of the asymptotic values that is Gaussian. Since the growing of PE is exponential and it is not affected by other parameters, it can be related to a spurious capacitance in the ROIC that charges during the first stages of the acquisition process.

The statistical differences in the parameters can be correlated with their position on the image frame. Figure 6 shows pictures of the frame used to perform the analyses in false colours, but the value of the pixels is substituted with the value of the fitting parameters of the same pixel. So we obtain a “spatial distribution” of the differences in the PE value and dynamics.

The dark blue circles areas in Fig. 6 are two illuminated regions on the images that have been removed prior to the dark analyses.

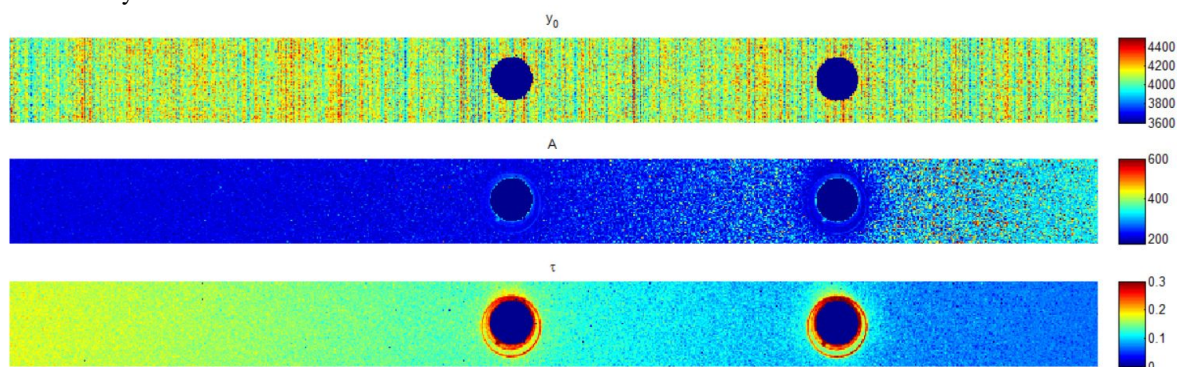


Fig. 6. Figure shows the distribution on one of the filters of STC of the fitting parameters (from top to bottom y_o , A , τ). The two blue areas are illuminated light spots not considered by the analysis.

It is worth to notice that no blooming or signal crosstalk (in y_o) is present in the areas close to the light-spots and so there is no apparent influence of the light on the PE of the nearby pixels, but there is a sort of blooming in A and τ parameters. It means that the final value of the PE does not seem dependent from the light, while the dynamics are slightly influenced.

Lets us suppose that the origin of the pedestal is not into the sensitive material but somewhere into the on-chip readout electronics. From these pictures we can infer that:

- The distribution of the PE follows the direction of the frame columns, as a sort of FPN.
- The amplitude A has higher values concentrated on the right of the image frame. That can explain the asymmetry of the peaks and the formation of the second peak at lower temperatures.

The exponential decay constant is distributed in different zones of the frames with values that increase, not uniformly, from right to left of the frame. Such a not uniformity in the values growth leads to the formation of the multi peak shape of its statistical distribution.

B. The Offset Peaks

The formation of an additional spurious signal layer on the picture makes more complicate the reconstruction of the real DN signal: that is the one generated by photons interaction.

Moreover, the signal feature that we will start to analyse in these paragraphs is not stable, as the pedestal, but it can change with different procedures to acquire the pictures. We named this effect from its shape in the images sequences, Peak Offset (PO).

Considering again Fig. 3, and taking into account the peak effect, we can assume as a hypothesis that the main PO signal is generated during the time elapsed between the acquisition of two successive two images (for a nominal acquisition set the repetition time). After its formation, its decay it is due to a low ability to reset the signal.

There is only one hardware procedure, i.e. the RESET, to discharge the sensitive area from all the photon-generated (and none) charges. This fact let us suppose that one of the main parameters to be considered for the PO dynamics is the time elapsed from the RESET to the image acquisition (or start), which coincides for low ITs to the Repetition Time (RT).

Peaks shown in Fig. 3 are the results of set of 15 images acquired with the same repetition time, while the first image of the set has been acquired after a waiting time greater than the RT.

To start studying the peak formation, only the first and last images of each set will be taken into consideration. This choice is to avoid the influence of the decrease of the signal values due to the following images, which can be considered as transitory. Different tests were performed varying the integration time IT and the time between the acquisition of the images, that is RT. That corresponds, in Fig. 3, to consider the effective RT for the last image of each set and the time elapsed between the acquisitions and the one immediately before as RT for the first image of each set (the one with the peak signal).

We decided to adopt a three-dimensional visualization inserting in a 3D graph the DN of a reference pixel vs the Integration time (IT) and the time between two resets (RT). The set of images considered includes the first frame (i.e. the one with the peak) and the last frame of each set (i.e the one in which the signal is supposed to be stable). The other images are not taken in account as their signal value are considered transient. The result is shown in Fig. 7.

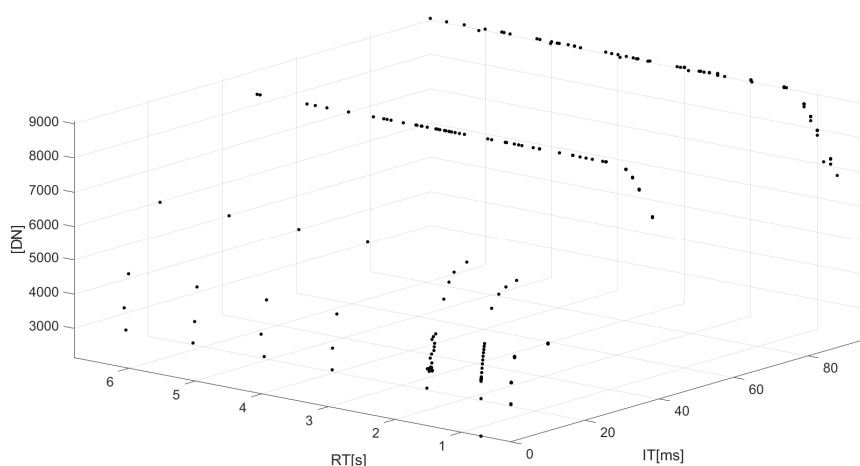


Fig. 7. The picture shows the value of a reference pixel plotted vs the integration time and the repetition time. The measurements are performed at ambient temperature (292K).

Test demonstrates an expected behaviour for the dark for a minimal RT (250 ms) defined by the PE and a linear increase of the dark for higher values of IT. Moving along the RT axis the PE curves increase. For very high RT, this curve loses its dependence from the RT reaching a stable but very high (in terms of dynamic) curve.

In this graph the minimum value is always above 3000-4000 DN, so all these pictures are affected by the PE effect. About the PO effect, it is clear that it can be charged both during the IT and during the time elapsed between two image sets. It is unusual that the two charging time constants seem to be really different since the two horizontal axis are expressed in different units (ms and s, a difference of three order of magnitude). This suggests there are two different effects charging the PO.

An example of the different dark behaviour wrt the RT is shown in Fig. 8 where the data are interpolated with a double exponential fit for better visibility.

The red curve represents the minimum dark signal curve measured with a RT of 250 ms (this limit is imposed by image read out and the compression). The PE (measured in this test to be around 4700 DN) increases with the repetition time reaching 6390 DN for a RT of 700 ms. All the cases in which the RT is greater than 1.5 s are characterized by the same curve overlapped. This is what we can call ‘‘Saturation zone of the RT’’.

Considering that STC nominal RT (during Global Mapping phase) will be between 7 and 13 s (depending on the latitude of the S/C), in this region the dark is not sensible to the time between two images and so it can be calibrated as a function of the pure IT even if it covers half the sensor dynamics.

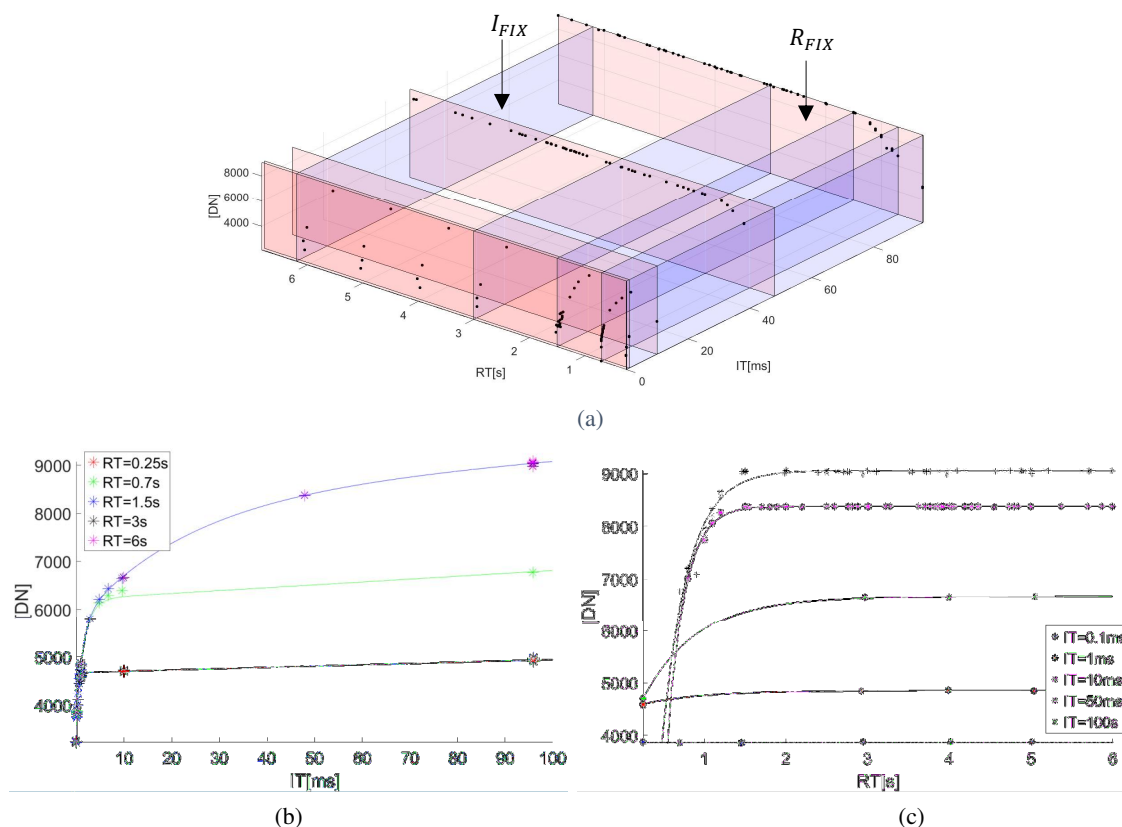


Fig. 8. In (a) the data set is shown with the slices representing the curves derived considering the dependence only from IT with a fixed RT (in blue) and the vice versa (in red). Slices defined by a fixed repetition time are indicated with R_{FIX} , the orthogonal ones with I_{FIX} . In (b) the dark curve for some fixed RT are presented. Curves (representing a double exponential approximation of the dataset) with a RT > 1.5s are overlapped. In (c) trends with a fixed IT are shown all fitted with the exponential model proposed in Eq (1).

V. CONCLUSION

In this paper the analyses of the calibration of the dark current of the STC CMOS detector are presented. Unexpected phenomena, affecting these measurements, have been found.

In particular two different contributions have been identified in the signal, measured by the sensor in dark. The first of them is the presence of an offset that builds up in the first 0.4 ms of the IT. Such a pedestal is not linear with the integration time but it can be modelled with an exponential which has a fixed temporal constant (depending on the temperature).

The second effect can be seen at longer integration times. It builds up during the interval between two images and during the integration time, but it is discharged by sequences of images with high repetition rate. This charging effect reaches a saturation level for RTs greater than 1.5 s or for ITs < 0.5 ms for the measurements done with the detector at room temperature.

Even if the causes of these issues are still to be understood, both can be characterised and partially calibrated in order to mitigate their effects on the in flight measurements.

The analysis of all the images acquired so far, which have been taken at different detector temperatures, permitted us to extrapolate the effect of PO and PE at the nominal operative detector temperature (268K). The results of this analysis allow to predict the minimum impact on the scientific images to be acquired during the BC mission lifetime.

The two different observing strategies (with different objectives) which will be carried out with STC have to be considered: the global mapping of the Mercury surface, which will allow to derive a global DTM, and the colour mapping of selected areas. In the global mapping phase (acquisitions with high RT and low IT) the sensor will work in the saturation zone of the RT and the dark signal will be defined for each pixel as a function only of the IT. This implies losing at least 4500 DN, i.e. 27% of the dynamic range. In the colour mapping phase (acquisition with low RT and high IT) the DSNU is a function of both the IT and the RT and the expected reduction in the dynamical range will be higher than 40%. These considerations are obviously made assuming that the RT and IT limits defined are constant with respect to the temperature.

To assess the detector issues and validate the way to deal with them, some tests at the detector nominal operative temperature are foreseen to be done in the Near Earth Commissioning Phase just after launch in 2018.

ACKNOWLEDGMENTS

The authors wish to thank the SIMBIO-SYS prime contractor Leonardo S.p.A (Campi di Bisenzio (FI) – Italy). This activity has been realized under the BepiColombo Agenzia Spaziale Italiana (ASI) contract to the Istituto Nazionale di Astrofisica (INAF I/022/10/0) .

REFERENCES

- [1] J. Benkhoff, J. van Casteren, H. Hayakawa, M. Fujimoto, H. Laakso, M. Novara, P. Ferri, H. R. Middleton and R. Ziethel, “BepiColombo - Comprehensive exploration of Mercury: Mission overview and science goals”, *Planet. Space Sci.*, vol. 58(1-2), pp. 2-20, 2010.
- [2] J. Benkhoff, “The BepiColombo Mission to explore Mercury - Overview and mission status”, *44th LPSC*, 2834, 2013.
- [3] E. Flamini, et al., “SIMBIO-SYS: The spectrometer and imagers integrated observatory system for the BepiColombo planetary orbiter”, *Planet. Space Sci.*, vol. 58, pp. 125-143, 2010.
- [4] V. Da Deppo, G. Naletto, G. Cremonese, and L. Calamai, “Optical design of the single-detector planetary stereo camera for the BepiColombo European Space Agency mission to Mercury”, *App. Opt.*, vol. 49(15), pp. 2910-2919, 2010.
- [5] V. Da Deppo, G. Cremonese, G. Naletto, “Ghost images determination for the stereoscopic imaging channel of SIMBIOSYS for the BepiColombo ESA mission”, *Proc. SPIE*, vol. 8167, 81671U, 2011.
- [6] R. E. Mills, J. J. Drab, and A. Gin, “Advanced staring Si PIN visible sensor chip assembly for Bepi-Colombo mission to Mercury”, *Proc. SPIE*, vol. 7439, 74390A, 2009.
- [7] L. Colangeli, et al., “The High Resolution Imaging Channel of the SIMBIO-SYS instrument on board the BepiColombo mission to Mercury”, *37th COSPAR Scientific Assembly*, vol. 37. 2008.
- [8] L. Gambicorti, et al.. “The CaSSIS imaging system: optical performance overview”, *Proc. SPIE*, vol. 9904, 99041E, 2016.
- [9] V. Da Deppo, et al., “Radiometric model for the stereo camera STC onboard the BepiColombo ESA mission”, *Proc. SPIE*, vol. 9911, 99111T, 2016.
- [10] E. Simioni, et al., “Geometrical distortion calibration of the stereo camera for the BepiColombo mission to Mercury”, *Proc. SPIE*, vol. 9904, 990410, 2016.
- [11] E. Simioni , C. Re , V. Da Deppo, G. Naletto, D. Borrelli , M. Dami , I. Ficai Veltroni , G. Cremonese , “Indoor calibration for stereoscopic camera STC, a new method”, *ICSO2014 - International Conference on Space Optics*, Tenerife, 7-10 October, 2014.
- [12] C. Re ,E. Simioni, G. Cremonese , R. Roncella , G. Forlani , Vania Da Deppo , G. Naletto , G. Salemi, “DTM generation from STC-SIMBIO-SYS images”, *Proc. SPIE*, vol. 9528, 2015.
- [13] V. Da Deppo, G. Naletto, G. Cremonese, L. Calamai, R. Paolinetti, S. Debei and E. Flamini, “Optical design performance of the stereo channel for SIMBIOSYS onboard the BepiColombo ESA mission”, in *Proceeding of the 8th International Conference on Space Optics*, Rhodes - Greece, 4-8 October 2010, 2010.
- [14] A. De Groof, et. al., “CMOS-APS detectors for solar physics: lessons learned during the SWAP preflight calibration”, *Solar physics*, vol. 249(1), pp. 147-163, 2008.